ORIGINAL PAPER

A New Rock Brittleness Index Based on the Characteristics of Complete Stress–Strain Behaviors

Zhihao Kuang[1,2] · Shili Qiu[1] · Shaojun Li[1] · Shihui Du[3] · Yong Huang[3] · Xingqiang Chen[3]

Abstract
Rock brittleness is an essential mechanical property, which plays a significant role in rock classifications and rockburst risk evaluations. To overcome the problems associated with the traditional brittleness indexes not comprehensively charaterizing the rock strength and deformation behaviors, this study systematically summarized the existing rock brittleness indexes. Then, a novel brittleness index (BICSS) based on the complete stress–strain curves of rock under different confining pressures was proposed. Its advantages included innovatively considering the characteristic stresses and strains at the stage of crack initiation, the peak points, and residual points. The index also described the stress growth rates from the pre-peak crack-initiation stress to the peak stress points, as well as the stress drop rates from the peak stress to the residual stress points. This study conducted uniaxial and triaxial compression tests of metamorphic sandstone, granite, and gneiss obtained from a deeply buried long-line tunnel group. The aforementioned tests were combined with wave velocity tests and thin-section identification tests using polarizing microscopy techniques. The reliability and applicability of the index were then successfully verified. The results showed that the BICSS could not only quantify and classify the brittleness characteristics of different rock types and characterize the confining pressure inhibition behaviors of rock brittleness, but could also comprehensively express the influences of homogeneity, mineral compositions, and particle sizes on the rock brittleness. Finally, through the parameter sensitivity analysis of the BICSS, the influences of subjective errors in the results of the cracking initiation stress and strain values caused by the different selections during the linear elastic phase could be successfully excluded, resulting in the further verification of the stability of the BICSS.

List of Symbols

a_i	Weight coefficient of brittle mineral type
a_j	Weight coefficient of each mineral
B_i	Brittleness index
C	Content of carbonate
Cl	Content of clay
Dol	Content of dolomite
E	Elasticity modulus
K_{ac}	Stress slope of the post-peak
Lm	Content of limestone
M	Post-peak modulus
M_i	Brittle mineral content
M_j	Each mineral content
Q	Content of quartz
Toc	Content of organic matter
W_{el}	Elastic energy at the peak stress point
W_{tot}	Total fracture energy
α	Standardized coefficients
β	Standardized coefficients
ε_{BRIT}	Peak strain
ε_{ci}	Crack initiation strain
ε_c^p	Plastic strain necessary for cohesion loss
ε_{el}	Elastic strain at the pre-peak stage of stress–strain curves
ε_f^p	Plastic strain necessary for frictional strengthening
ε_m	Reference value of the maximum peak strain

✉ Shaojun Li
sjli@whrsm.ac.cn

1   State Key Laboratory of Geomechanics and Geotechnical Engineering, Institute of Rock and Soil Mechanics, Chinese Academy of Sciences, Wuhan 430071, Hubei, China

2   University of Chinese Academy of Sciences, Beijing 100049, China

3   China Railway Frist Survey and Design Institute Group Co. Ltd., Xi'an 710043, Shaanxi, China

ε_n	Reference value of the minimum peak strain
ε_p	Peak compressive strain
ε_r	Residual compressive strain
ε_{tot}	Total strain at the pre-peak stage of stress–strain curves
η	Standardized coefficients
θ	Internal friction angle
μ	Mean value
υ	Passion ratio
ρ	Density
σ	Standard deviation
σ_3	Confining pressure
σ_c	Uniaxial compressive strength
σ_{ci}	Crack initiation stress
σ_p	Peak compressive strength
σ_r	Residual compressive strength
σ_t	Splitting tensile strength

1 Introduction

Brittleness is a crucial property of rock formations, particulary deeply buried rock formations. The research regarding brittleness is of major significance for deep rock mass engineering construction projects and disaster prevention measures. However, there is no universally accepted definition for rock brittleness. Morley (1944) and Hetenyi (1950) defined brittleness as the lack of material plastic. Howall (1960) proposed that brittleness is a manifestation of rock fractures accompanied by small plastic deformations. Ramsey (1968) argues that brittle failures occur when the rock cohesion has been destroyed. Obert and Duvall (1967) selected cast iron and rock as research objects, and then defined brittleness as the property of stress when it reached or slightly exceeded the yield strength. In another related study, Hucka and Das (1974) analyzed the concept of brittleness and pointed out that with increases in brittleness in rock material, the following phenomena can be observed: (1) Low-value elongation; (2) fracture failures; (3) formations of fine lines; (4) higher ratio of compressive to tensile strength; (5) higher resilience; (6) higher angles of internal friction; and (7) formation of cracks within indentations. Li et al. (2012) held that brittleness is a comprehensive property which can be used to describe the ability of rock material to develop from local damages to space fractures. These types of local damages are caused by uneven distributions of internal stress, which may result from the inhomogeneity of the mineral compositions. In other words, brittle rock is prone to sudden fractures under external forces and produces only minor inelastic deformations.

In rockburst risk assessments, the brittleness index is important for predicting potential rockburst disasters. Such disasters are known to be directly related to brittle fracturing

of rock masses and the stability of the surrounding rock structure. Meanwhile, the brittleness index is also an indispensable tool for rock mass classifications, as well as in the identification of possible failure characteristics. Since the early research regarding rock brittlenss was presented, Chinese and international researchers have proposed various quantitative expressions of rock brittleness from different perspectives, such as the inherent characteristics of the rock, complex external environmental conditions, and construction factors, including the rock strength parameters (George 1995; Altindag 2002, 2008; Yagiz 2009; Rickman et al. 2008); mineral compositions (Jarvie et al. 2007; Wang and Gale 2009; Buller et al. 2010); and the stress–strain curves of the rock brittleness characteristics (Hucka and Das 1974; Coates and Parsons 1966; Bishop 1967; Hajiabdolmajid and Kaiser 2003; Wang et al. 2014; Li et al. 2012; Tarasov and Potvin 2012, 2013; Meng et al. 2015; Xia et al. 2017; Chen et al. 2019), as detailed in Table 1. Among the aforementioned brittleness indexes, the index based on the stress–strain curves of rock formations is considered to be the one most commonly used in rock mechanics.

It was found in this study that, due to the diversity of the rock brittleness definitions and the complexity of rock engineering processes, the current evaluation methods for rock brittleness are varied. In addition, these brittleness evaluation methods originate from their own engineering backgrounds. Therefore, they tend to have strong pertinence, but poor adaptability. In previous studies conducted by Bishop (1967), it was pointed out that rock brittleness is closely related to the magnitudes of the post-peak stress or strain declines. In the aforementioned study, the corresponding brittleness indicators $\left(B_{14} = (\varepsilon_p - \varepsilon_r)/\varepsilon_p \quad B_{15} = (\sigma_p - \sigma_r)/\sigma_p\right)$ were established. However, with the increases in confining pressure, it was found that the values of parameters in the above indexes all increased in varying degrees. Therefore, it was concluded that it may be insufficient to use the decreases of the stress or strain levels alone as the evaluation indexes of rock brittleness. In the pre-feasibility study stage, people hope to have a comprehensive understanding of rock mass brittleness at the filed site, and then formulate effective prevention countermeasures, reasonable adjustments, and optimization designs for the excavation support and construction design of the high brittle rock mass construction section, which has great engineering and scientific research significance for reducing the loss of human and material resources caused by rockburst and spalling hazards. To address these issues, this study proposed a new type of brittleness index (BICSS), which takes into account the full stress–strain curves. The proposed index considers the stress growth rate from the crack-initiation stage to the peak point, as well as the stress drop rate from the peak point to the residual stage. During this study's investigation, a series of uniaxial and triaxial

Table 1 Summary of the most commonly used brittleness indexes

Classification	Brittleness index	References
Based on strength parameters	$B_1 = \sigma_c/\sigma_t$ $B_2 = (\sigma_c - \sigma_t)/(\sigma_c + \sigma_t)$	Hucka and Das (1974)
	$B_3 = \sigma_c \sigma_t/2$ $B_4 = \sqrt{\sigma_c \sigma_t/2}$	Altindag (2002, 2008)
	$B_5 = 0.198\sigma_c - 2.174\sigma_t + 0.913\rho - 3.807$	Yagiz (2009)
	$B_6 = [(E - E_{min})/(E_{max} - E_{min}) + (u - u_{min})/(u_{max} - u_{min})]/2$	Rickman et al. (2008)
Based on mineral composition	$B_7 = Q/(Q + C + Cl)$	Jarvie et al. (2007)
	$B_8 = (Q + Dol)/(Q + Dol + Lm + Toc + Cl)$	Wang and Gale (2009)
	$B_9 = \left(\sum_{i=1}^{m} a_i M_i\right)\Big/\left(\sum_{j=1}^{m} a_j M_j\right)$	Buller et al. (2010)
Based on stress–strain curves	$B_{10} = \sin\theta$ $B_{11} = W_{el}/W_{tot}$	Hucka and Das (1974)
	$B_{12} = \varepsilon_{el}/\varepsilon_{tot}$	Coates and Parsons (1966)
	$B_{13} = (\sigma_p - \sigma_r)/\sigma_p$ $B_{14} = (\varepsilon_p - \varepsilon_r)/\varepsilon_p$	Bishop (1967)
	$B_{15} = /(\varepsilon_f^p - \varepsilon_c^p)/\varepsilon_c^p$	Hajiabdolmajid and Kaiser (2003)
	$B_{16} = 8\sigma_c/\sigma_{ci}$ $B_{17} = \sigma_c \sigma_{ci}/16$ $B_{18} = \sqrt{\sigma_c \sigma_{ci}/16}$	Wang et al. (2014)
	$B_{19} = (\varepsilon_{BRIT} - \varepsilon_n)/(\varepsilon_m - \varepsilon_n) + \alpha CS_{BRIT} + \eta$	Li et al. (2012)
	$CS_{BRIT} = (\sigma_p - \sigma_r)/\left[E_p(\varepsilon_r - \varepsilon_p)\right]$	
	$B_{20} = (M - E)/M$ $B_{21} = E/M$	Tarasov and Potvin (2012, 2013)
	$B_{22} = \left[(\sigma_p - \sigma_r)/\sigma_p\right](lg|K_{ac}|/10)$	Meng et al. (2015)
	$B_{23} = (\sigma_p - \sigma_r)/(\varepsilon_r - \varepsilon_p) + (\sigma_p - \sigma_r)(\varepsilon_r - \varepsilon_p)/(\sigma_p \varepsilon_p)$	Xia et al. (2017)
	$B_{24} = (\sigma_p - \sigma_{ci})/[\sigma_p(\varepsilon_p - \varepsilon_{ci})] + (\sigma_p - \sigma_r)/[\sigma_p(\varepsilon_r - \varepsilon_p)]$	Chen et al. (2019)
	$B_{25} = \left[(\sigma_p - \sigma_{ci})\varepsilon_p\right]/\left[\sigma_p(\varepsilon_p - \varepsilon_{ci})\right] + (\sigma_p - \sigma_r)\varepsilon_p/\left[\sigma_p(\varepsilon_r - \varepsilon_p)\right]$	Chen et al. (2018)

compression tests were performed on metamorphic sandstone, granite, and gneiss samples. The tests were combined with wave velocity tests and thin-section identification tests using polarizing microscopy techniques. Subsequently, the change law of rock brittleness was analyzed, and the rationality and reliability of the proposed BICSS index were verified. The results showed that the BICSS was superior to previous indicators in quantifying and classifying the brittleness characteristics of different types of rock, and also in characterizing the inhibition effects of confining pressure on rock brittleness. The BICSS was also able to accurately describe the influence effects on the rock brittleness of the weathering degrees, homogeneity, mineral compositions, particle sizes, and cementation structures.

2 Brittleness Index Calculation Method

Rock is a natural heterogeneous material, which is mainly manifested in the uneven distribution of rock mineral composition, particle size, and mineral particle structure in different directions. Therefore, under the action of external force, the local stress concentration phenomenon will appear in the primary cracks, micro-voids, and particle boundaries within the rock. When the local stress exceeds the strength of the grains, then local failure of the rock will occur, which is manifested as a rock crack initiation in the macroscopic view. When a crack appears in the rock, then the stress concentration phenomenon will transfer to the crack tip, which will promote the crack propagation and eventually lead to the split failure of the rock. Wang et al. (2014) believes that the rock type, mineral composition, micro-cracks, and lattice defects in the rock can be characterized by the crack-initiation stress. Tarasov and Potvin (2013) suggested that when loading a rock specimen, the specimen deformation is always macroscopically stable and controllable, before the peak stress has been reached. Macroscopic instability associated with strength degradation in the form of spontaneous failure can only take place in the post-peak region. The post-peak instability can be treated as a manifestation of rock brittleness. According to the above analysis, in the study of rock brittleness, its controlling factors should be comprehensively considered, such as the damage evolution process of pre-peak microfracture, strength deterioration process caused by post-peak failure, and deformation evolution law. A great number of studies (Bishop 1967; Wang et al. 2014; Tarasov and Potvin 2012, 2013; Meng et al. 2015; Xia et al. 2017; Chen et al. 2019) have held that this process can be effectively characterized by the crack-initiation stress, peak stress, residual stress, and strain values of those corresponding characteristic stress points. Therefore, it was considered to be very important to consider these characteristic parameters when establishing this study's proposed brittleness index.

This study comprehensively considered the pre-peak and post-peak stages of the stress–strain curves. Then, a new rock brittleness evaluation index was proposed as follows:

$$BICSS = B_{p1} \times B_{p2}, \tag{1}$$

where B_{p1} is the pre-peak brittleness index; and B_{p2} indicates the post-peak brittleness index.

Based on the above analysis results and the summaries of typical rock stress–strain curves achieved by the existing brittleness indexes, the curves were divided into six categories, as shown in Fig. 1.

As illustrated in Fig. 1a, the peak point strain and the stress drop rate from the peak point to residual stage (hereinafter referred to as the post-peak stress drop rate) were the same. However, it can be seen in the figure that the stress rise rate from the pre-peak crack-initiation stage to the peak point (hereinafter referred to as the pre-peak stress rise rate) of Sample #2 was larger than that of Sample #1. Therefore, the brittleness of the rock represented by Sample #2 was higher than that of Sample #1. In Fig. 1b, only the post-peak stress drop rate was the same. Although the pre-peak stress rise rate of Sample #2 was higher than Sample #1, the peak point strain of Sample #1 was smaller than that of Sample #2. Therefore, it was difficult to directly compare the brittleness differences between the two samples.

Furthermore, based on the above analysis results, it was believed in this study that the definition of the pre-peak brittleness index should contain two important parameters as follows: (1) the pre-peak stress rise rate and (2) the peak strain. Under the same stress growth conditions, the higher the pre-peak stress rise rate, the smaller the deformations of the rock from crack initiation to penetration. In addition, the peak strain will represent the relative magnitude of inelastic deformations of the rock failure mode. Therefore, by combining the above with the accepted definition of brittleness, it was clear that rock brittleness was proportional to the rate of pre-peak stress rise, and inversely proportional to the peak strain value. Therefore, the brittleness index of the pre-peak stress–strain curves could be defined as follows:

$$B_{p1}^* = \frac{\sigma_p - \sigma_{ci}}{\varepsilon_p(\varepsilon_p - \varepsilon_{ci})}. \tag{2}$$

Similarly, through the analysis of the data shown in Fig. 1c, d, the brittleness index of the post-peak stage was obtained as follows:

$$B_{p2}^* = \frac{\sigma_p - \sigma_r}{\varepsilon_p(\varepsilon_p - \varepsilon_r)}. \tag{3}$$

In the next step of the current study, the rationality of the proposed index was verified by the results, as shown

in Fig. 1e, f. As can be seen in Fig. 1e, Samples #1 and #2 had displayed the same peak strain values. Meanwhile, the pre-peak stress rise rate and post-peak stress drop rate of Sample #2 were found to be greater than those of Sample #1. It was not difficult to see that the brittleness of Sample #2 was higher than that of Sample #1. It can be seen that the two samples shown in Fig. 1f had the same stress rise and drop rate. However, the peak strain value of Sample #1 was smaller than that of Sample #2. Therefore, the rock brittleness represented by Sample #1 was higher. These results indicated that the brittleness index based on the pre-peak and post-peak stage proposed in this study could comprehensively and reliably evaluate the brittleness characteristics of rock formations.

Considering that rock mass lithology and in situ stress state will not change greatly during the majority of construction processes, it has been found to be unreliable for engineering guidance procedures to use the comparative results of rock brittleness evaluations from different areas. Therefore, any newly defined rock brittleness index should include absoluteness. When an index is used to evaluate the brittleness of a certain type of rock, the calculated values should be able to directly reflect the brittleness of that particular type of rock without comparing it with other rock types. Therefore, to solve this problem, the pre-peak and post-peak brittleness indexes were normalized in the present study as follows:

$$B_{p1} = 1 - e^{-\frac{\sigma_p - \sigma_{ci}}{10\varepsilon_p(\varepsilon_p - \varepsilon_{ci})}} \quad B_{p2} = 1 - e^{\frac{\sigma_p - \sigma_r}{10\varepsilon_p(\varepsilon_p - \varepsilon_r)}}. \tag{4}$$

The brittleness index proposed in this study was able to take into account the stress rise rates from the pre-peak crack-initiation state to the peak point, as well as the stress drop rates after the peak point. At the same time, by considering the definition of brittleness, the peak strain value was taken as the control variable. Then, a brittleness index calculation method based on the entire process of the stress–strain curves was established. The method was found to have the advantages of high adaptability, high reliability, and easy acquisition of parameters.

3 Verification and Comparison of the Brittleness Indexes Using Experimental Testing Procedures

3.1 Experimental Procedures

Rock specimen size has a significant effect on the peak stress, peak strain, elastic modulus, and failure mode of the specimen (Yang et al. 2005; Komurlu 2018; Meng et al. 2016); therefore, it is necessary to study the brittle behavior of rock materials under the condition of standard size. In
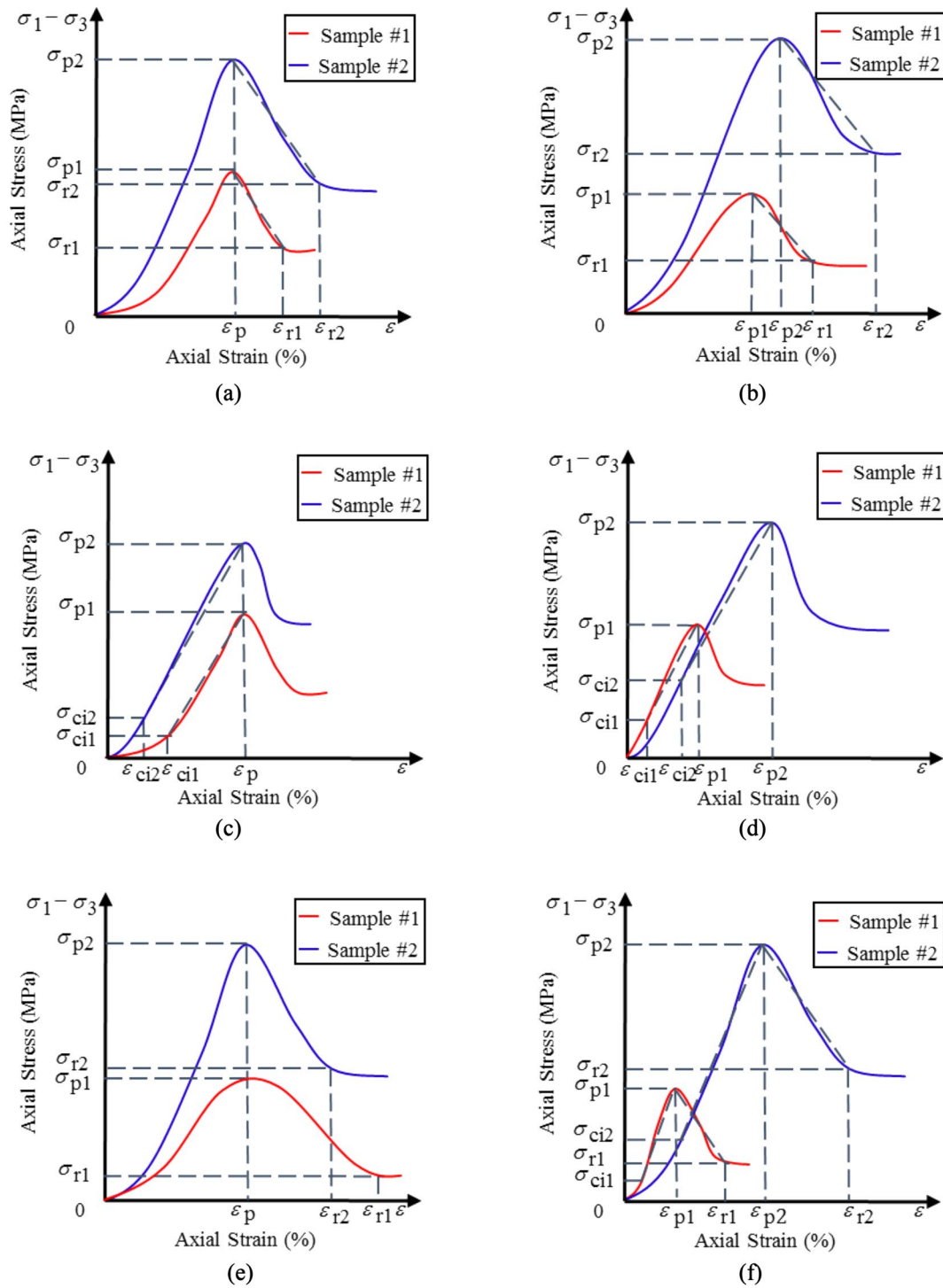
Fig. 1 Typical stress–strain curves for brittleness index illustrations. **a** Peak point of the strain and post-peak stress drop rate are the same, but the pre-peak stress rise rate was different; **b** pnly the post-peak stress drop rate was the same, and the pre-peak stress rise rate and peak point strain were different; **c** peak point strain and pre-peak stress rise rates are the same, but the post-peak stress drop rate is different; **d** only the pre-peak stress rise rate is the same, and the post-peak stress drop rate and peak point strain are different; **e** only the peak point strain is the same, and the post-peak stress drop rate and pre-peak stress rise rate are different; **f** pre-peak stress rise rate and the post-peak stress drop rate are the same, but the peak point strain is different

accordance with the method suggested by the International Society for Rock Mechanics (ISRM 1983; Fairhurst and Hudson 1999), standard cylindrical specimens measuring 100 mm in height and 50 mm in diameter were constructed from granite, metamorphic sandstone, and gneiss, as shown in Fig. 2. The two ends of each specimen were polished with a grinder to ensure that the parallelism error between the two ends of the specimens was less than 0.05 mm. Existing studies have shown that temperature has a great influence on the fracture mechanism of granite. When the external temperature reaches 300–600 ℃, then the friction between particles in granite (igneous rock) will increase, and the cohesive force at the grain boundary will be weakened, which will lead to plastic deformation in the granite (Gautam et al. 2018). Temperature has similar effects on the strength and deformation of marble (metamorphic rock) and sandstone (sedimentary rock) (Gautam et al. 2016, 2019). According to statistics, cutting tools and grinding tools will generate a great deal of cutting heat during the processing of hard rock. In general, the average working temperature of cutting tools and grinding tools is about 500 ℃. Therefore, it is necessary

Fig. 2 Conventional triaxial test rock samples. **a** Metamorphic sandstone samples; **b** Granite samples; **c** Gneiss samples

to control the temperature strictly during sample processing for subsequent brittleness research.

The processed samples were divided into three categories according to lithology. Due to the fact that the main lithology of the deep-buried long tunnel supported by this article is granite, the selected deep boreholes mainly exposed the granite strata. As there were no deep borehole core specimens for metamorphic sandstone and gneiss, the corresponding research on different overburden could not be carried out. The granite was subdivided into the following four grades: 150 m, 300 m, 450 m, and 600 m, respectively, according to the overburden. Each group contained five test samples and three candidate samples. Conventional triaxial tests were carried out using an MTS815.04 rock mechanics testing machine controlled by an electro-hydraulic servo system at the Wuhan Institute of Geomechanics, Chinese Academy of Sciences. The MTS815.04 test system is composed of loading part, testing part, and control part; its stiffness of load frame is 11.0×10^9 N/m; maximum allowable axial stress is 4600 kN; and maximum lateral pressure is 140 MPa. The test system can measure the axial and circumferential strain of the specimen. The measurement of axial deformation can be divided into two types, namely the linear variable differential transformer (LVDT) and strain gauge measurement method. Circumferential deformation can be measured with a circumferential extensometer. Prior to the test, the measuring device must be calibrated to ensure that the data measured during the test are accurate and objective. The calibration method is as follows: fix the micrometer on the movable end of the extensometer controlled by software; insert the gauge blocks of known specifications in turn; and then compare the value measured by the testing machine with the total gauge block specifications. If the error is less than 0.03%, then the calibration has been completed. For the rock triaxial test system, test deformation measuring device, and extensometer calibrator, please refer to Fig. 3. Generally speaking, the end effect, size effect, and stress concentration effect will inevitably be encountered in laboratory rock mechanics tests. However, strain gauges can effectively resolve the above problems, its main concept being to take a gauge length of 0.5 times the height of the sample in the middle of the sample as the measuring section, by which to measure the axial strain of the sample. However, under the condition of triaxial compression, due to the fact that the approximate location of the shear fracture surface cannot be predicted, and the measurement range of the strain gauge is limited, the measurement results cannot accurately reflect the deformation of the specimen. To resolve the above problems, the axial LVDT strain sensor can be added into the specimen deformation measuring device, and under the combined action of LVDT and strain gauge, the stress–strain curve of the specimen after failure can be measured more accurately. The circumferential deformation of the specimen
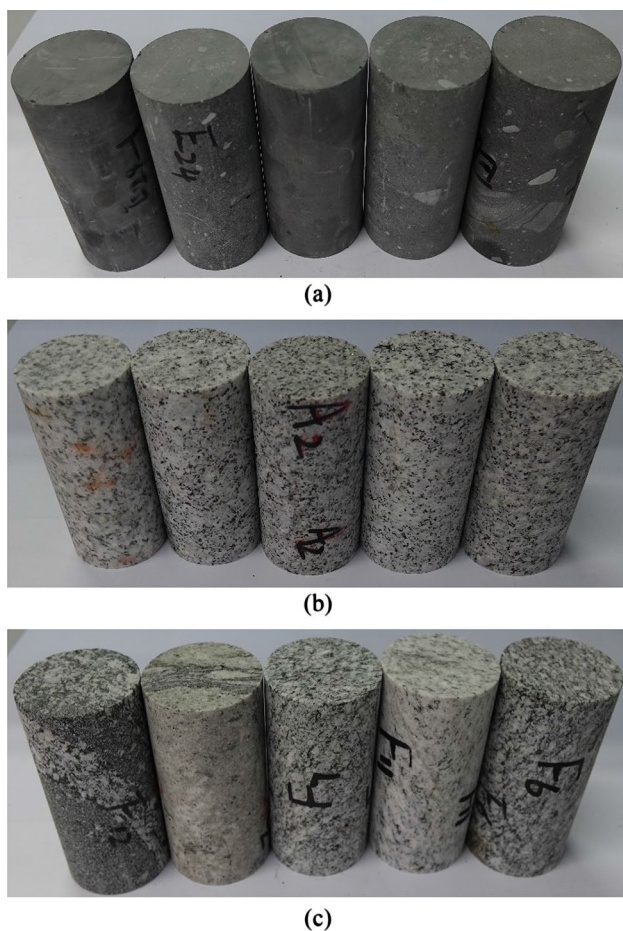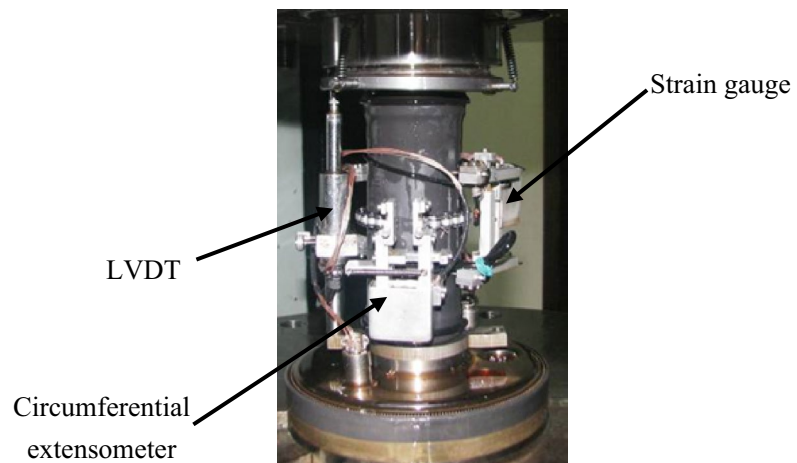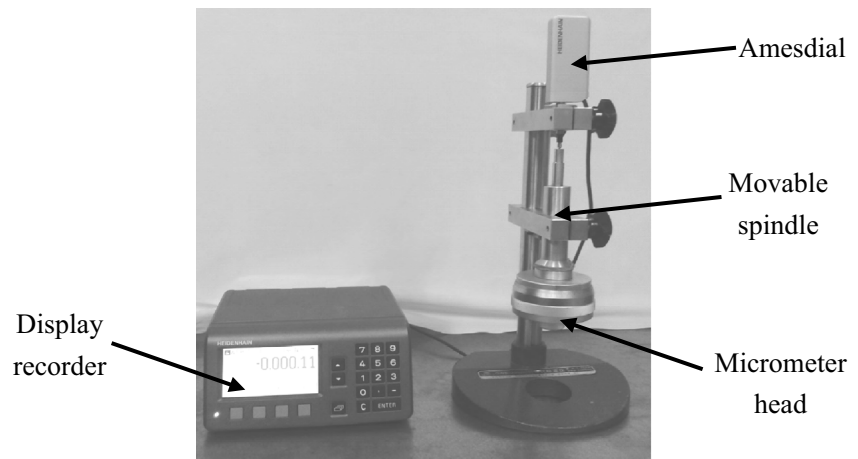
Fig. 3 MTS815.04 electro-hydraulic servo-controlled rock mechanics testing and the calibrator system: **a** the rock mechanical triaxial testing system; **b** the installation of deformation measurement sensors; **c** the extensometer calibrator

can be measured by the circumferential extensometer installed in the middle of the specimen.

Considering the in situ stress conditions of deep-buried tunnels, which shows that the principal stress variation range of the tunnel group is 0.6–43.3 MPa. Therefore, the maximum confining pressure grade of the triaxial test can be set to 40 MPa. In the process of tunnel excavation, the occurrence of free face will lead to the phenomenon of stress redistribution, stress concentrations in excess of the crack-initiation stress will cause local damage to the rock mass.

This degree of damage is very sensitive under low confining pressure conditions (Martin 1997). Therefore, it is necessary to set more intervals in the range of low confining pressure to study the change of rock brittleness. In summary, the confining pressure applied to specimens can be divided into five levels: 0, 5, 10, 20, and 40 MPa. To reduce the error caused by factors other than the nature of rocks, the specimens with abnormal results caused by man-made or machine faults in the test process should be supplemented in time with the candidate specimen. The test process is as follows:

(a) Before the test, carry out size measurement, sonic test, and take photos of the specimen in all directions. The purpose of acoustic testing is to screen out the samples in the same group with similar internal structure density, so as to reduce the test error caused by the internal factors of the specimens.

(b) The indenter is placed on both ends of the specimen, and then, the specimen is wrapped with a pyrocondensation pipe of 60 mm in diameter and 0.1 mm in thickness, and heated with a hot blast to make the pyrocondensation pipe and specimen fit tightly together.

(c) The axial stress and confining pressure were simultaneously loaded to the test setting confining pressure value, and then, the confining pressure was kept constant, using the LVDT axial displacement servo control method, and the loading rate was 1.0×10^{-3} mm/s, until the sample had broken.

(d) The test was ended, the specimen was removed, as was the pyrocondensation pipe, and the failure morphology of the specimen was recorded.

3.2 Verification and Comparison of the Evaluation Methods for Rock Brittleness Under Triaxial Compression Tests

3.2.1 Comparison of the Evaluation Methods for Rock Brittleness in Different Lithologies

According to the differences in lithology, the rock samples were divided into three groups: granite, metamorphic sandstone, and gneiss, with a bedding angle of approximately 60°. Then, conventional triaxial tests with different confining pressure grades were carried out. The test curves and failure morphology are shown in Fig. 4. It can be seen in the figure that, under uniaxial compression conditions, the yield stages in the axial stress–strain curves of the three groups of rock were not obvious. In particular, the metamorphic sandstone had basically presented linear elastic loading in the pre-peak stage, which then instantaneously dropped to approximately 0 MPa when the stress value reached its peak strength. In contrast, there was obvious weakening observed in the cohesive force and strengthening of the internal friction during

rock failures in the post-peak stage of the gneiss samples under uniaxial compression conditions. In terms of failure morphology, block ejection was observed in the metamorphic sandstone, and there were many vertical and oblique tension cracks on the surface. Small fragments could be seen on the surface of granite, and there were two intersecting main cracks. and the gneiss was basically destroyed along its bedding.

Under the action of confining pressure, the pore and fracture in the rock were compacted, which increased the friction between the fractures, and the strength and elastic modulus of the rock also increased correspondingly. Therefore, with the increase of confining pressure, the three groups of specimens showed higher peak strength, peak strain, and residual strength on the stress–strain curve. It is worth noting that metamorphic sandstone had a negative unloading modulus after the stress reaches the peak point under the condition of low confining pressure (5 MPa and 10 MPa); in other words, after the peak point, the axial strain in the stress–strain curve decreased with the decrease of stress. The occurrence of this phenomenon indicated that rock fragments would be ejected during the process of failure, and that this phenomenon would be suppressed as the confining pressure increased (Zhang and Li 2019). In terms of failure morphology, the three groups of specimens all produced shear cracks that formed a certain angle with the axial direction, and penetrated the specimen under the action of confining pressure. Among them, the shear failure plane which formed on the surface of metamorphic sandstone was similar to a shear zone, and the specimen divided into two parts by the macroscopic shear plane could be directly separated. The failure characteristics of granite under low confining pressure (5 MPa, 10 MPa) were similar to those of metamorphic sandstone; however, as the confining pressure increased, the two parts of the specimen divided by the macroscopic crack still bit together, and a large amount of white powder and granular debris produced by shear dislocation could be observed in the middle of the crack. The gneiss was destroyed along its bedding under uniaxial and triaxial conditions. However, it is worth noting that, under the condition of a confining pressure of 40 MPa, the shear crack at the bottom of the gneiss specimen coincided with its bedding plane. However, the cracks eventually formed not along the bedding plane, but penetrated from the middle of the specimen to the bottom, and the specimen on both sides of the macroscopic crack could not be completely separated.

It can be seen that, from the mechanical point of view, the formation, propagation, and penetration of cracks in the rock under uniaxial conditions are manifested as tensile failure, which was caused by the axial pressure reaching the cohesive strength of particles in the specimen. Under the action of confining pressure, when the axial pressure reached the cohesive strength of the particles and the micro-cracks were
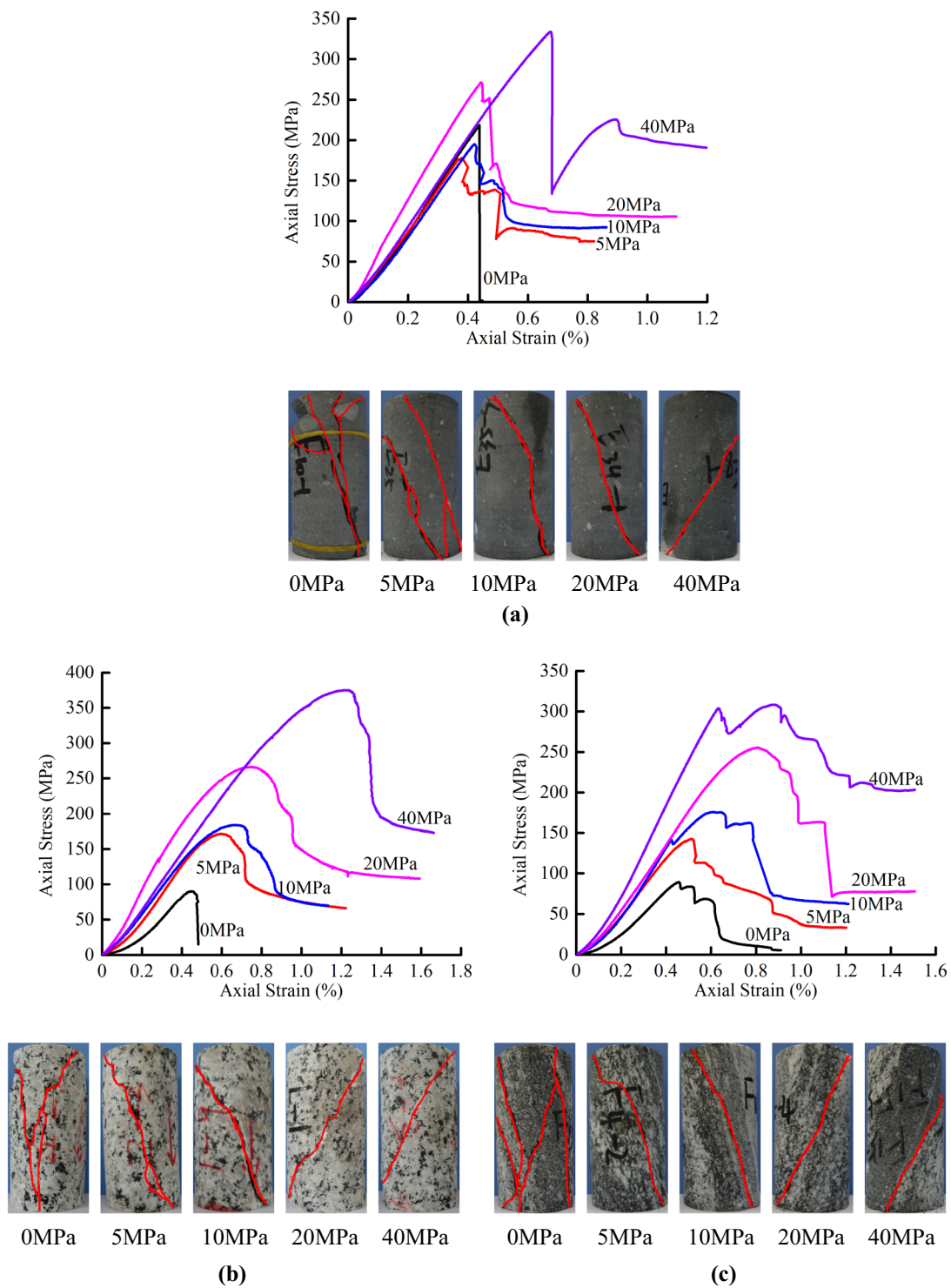
Fig. 4 Stress–strain curves and failure morphology of the three kinds of rock samples under conventional triaxial compression: **a** test curves and failure morphology of the metamorphic sandstone sam-ples; **b** test curves and failure morphology of the granite samples; **c** test curves and failure morphology of the gneiss samples

formed, then the friction on the surface of the crack was mobilized accordingly, and the bearing capacity of the specimen gradually decreased from cohesive strength to friction (residual) strength. In addition, from the perspective of rock failure mode, that is, from uniaxial to triaxial conditions, the rock failure mode changed from tension to shear.

The crack-initiation stress parameters of the brittleness index proposed in this study were determined using the crack volume strain inflection point method proposed by Martin (1997). The characteristic stress and strain values which were determined according to the test curves are shown in Table 2. The test data were calculated using the proposed BICSS, along with the brittleness indexes which are commonly used in China and internationally. The results are detailed in Fig. 5. It can be seen in the figure that, under the uniaxial compression conditions, the brittleness evaluation results were consistent with each brittleness index. That is to say, the metamorphic sandstone samples had the highest

Table 2 Result of the triaxial compression tests of the rock samples with different lithologies

Lithology	σ_3 (MPa)	σ_{ci} (MPa)	ε_{ci} (10^{-3})	σ_p (MPa)	ε_p (10^{-3})	σ_r (MPa)	ε_r (10^{-3})	B_{13}	B_{22}	B_{23}	B_{24}	B_{25}	BICSS
Metamorphic sandstone	0	66.53	0.47	218.6	4.39	1.75	4.4	0.992	0.435	24,093	110.39	484.22	0.587
	5	78.79	0.35	178	3.81	84.6	5.09	0.525	0.098	72.988	0.571	2.172	0.452
	10	94.74	0.7	195.07	4.23	100.05	5.47	0.487	0.092	76.317	0.536	2.267	0.409
	20	115.61	0.28	271.28	4.44	107.61	8.1	0.603	0.100	45.220	0.303	1.346	0.361
	40	82.95	0.41	333.68	6.76	207.65	9.17	0.378	0.065	52.596	0.275	1.863	0.238
Granite	0	24.947	0.960	89.593	4.468	15.257	4.817	0.830	0.193	212.85	2.581	11.531	0.335
	5	41.816	0.805	171.31	4.817	94.223	7.747	0.450	0.064	26.590	0.342	1.647	0.205
	10	50.714	0.587	183.84	6.666	87.873	8.812	0.522	0.086	44.898	0.362	2.416	0.137
	20	61.702	0.597	266.18	7.432	118.96	12.160	0.553	0.083	31.491	0.229	1.705	0.113
	40	57.497	0.546	374.93	12.323	185.41	14.642	0.505	0.097	81.831	0.290	3.572	0.095
Gneiss	0	40.30	1.75	89.40	4.56	17.44	6.70	0.805	0.123	34.025	0.572	2.609	0.166
	5	46.12	0.91	142.44	5.11	50.84	8.81	0.643	0.090	25.165	0.334	1.707	0.139
	10	55.21	1.04	175.83	6.10	67.10	9.87	0.618	0.090	29.218	0.300	1.827	0.122
	20	51.81	0.71	255.43	8.08	77.07	13.08	0.698	0.108	36.113	0.248	2.003	0.103
	40	50.29	0.67	308.26	8.74	202.71	13.94		0.045	20.477	0.170	1.481	0.063

In the table, σ_3 denotes the confining pressure; σ_{ci}, σ_p, σ_r and ε_{ci}, ε_p, ε_r represent the crack initiation stress, peak compressive strength, residual compressive strength, and the strain value of the corresponding stress, respectively; B_{13}, B_{22}, B_{23}, B_{24}, and B_{25} refer to the brittleness indexes which are commonly used in China and internationally
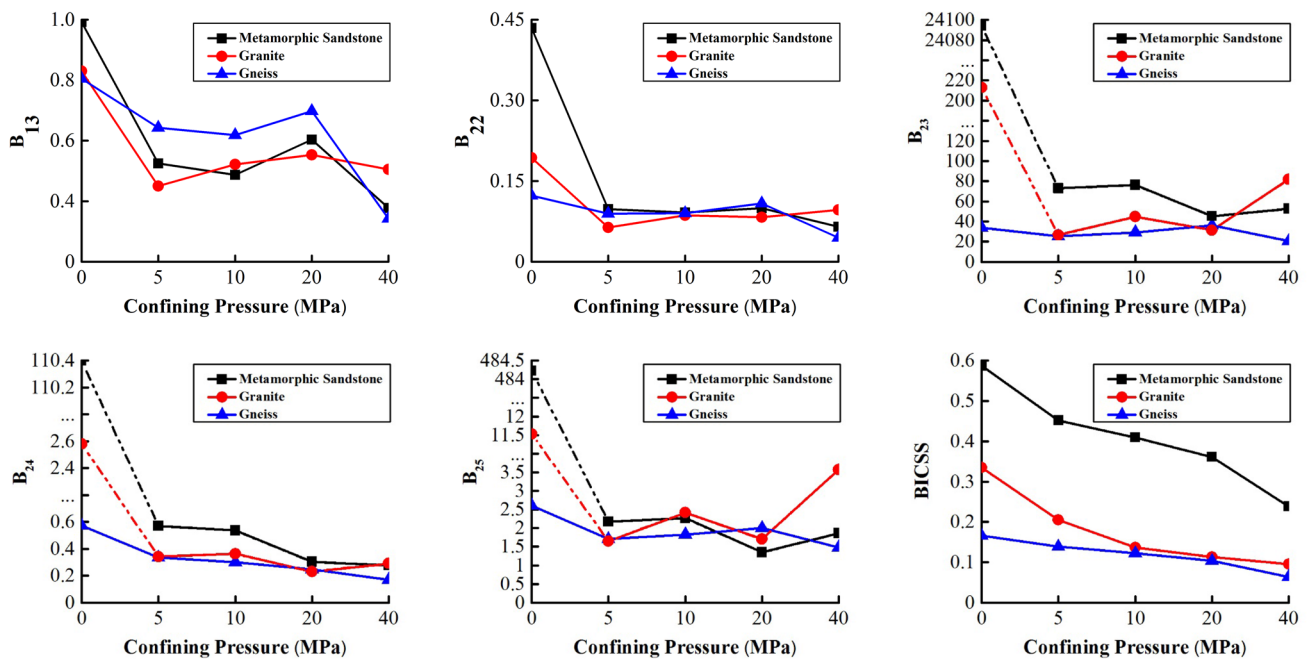

Fig. 5 Calculation results of the typical brittleness indexes

brittleness, and the gneiss brittleness was the lowest of the tested samples. However, under the effects of increased confining pressure levels, the results of evaluations of each brittleness index were found to vary. For example, when combined with the stress–strain curves of the examined rock, it was found that the metamorphic sandstone was basically in a linear elastic stage before the peak occurred, and the peak strain had been lower than that of granite and gneiss. Upon further examination, it was observed that the peak strain had rapidly fallen after the peak, and there was a rebound process observed after the peak stress drop at 40 MPa confining pressure. It was ascertained from the above-mentioned analysis results that the brittleness of the metamorphic sandstone under confining pressure levels of 0 MPa, 5 MPa, 10 MPa, and 20 MPa was potentially the largest of the three lithologic rock groups. However, the compression test results under a confining pressure of 40 MPa could not be simply compared using the test curves and failure morphology. The calculation results of the B_{13}, B_{22}, and B_{25} methods showed that the brittleness of the granite and gneiss was higher than that of the metamorphic sandstone under 5 MPa, 10 MPa, and 20 MPa confining pressure, which was inconsistent with the aforementioned analysis results. Therefore, those three brittleness evaluation methods were concluded to be unsuitable for the brittleness evaluations of different lithologic rock specimens under triaxial conditions.

Under the condition of a confining pressure of 40 MPa, the post-peak drop rate of granite was larger than that of metamorphic sandstone. For example, the axial stress of the granite decreased by 189.52 MPa during an axial strain increase of 0.0023, and the axial stress of the metamorphic sandstone decreased by 125.03 MPa during an axial strain increase of 0.0024. These results explained the observed phenomenon that the brittleness of the granite was greater than that of metamorphic sandstone calculated by the B_{23}. From the pre-peak stage, the peak stress and strain values of the granite were larger than those of the metamorphic sandstone. This was particularly evident for the peak strain values, which were observed to be nearly twice as much as that of metamorphic sandstone. Meanwhile, the effects of peak strain on rock brittleness had been neglected by B_{23} and B_{24}. Therefore, the results of this study's brittleness evaluation methods B_{23} and B_{24} were found to be unreliable for accurately evaluating the brittleness of rock under high confining pressure. The results of the BICSS calculations indicated that the brittleness of the metamorphic sandstone was much larger than that of the granite and gneiss under the various confining pressure conditions. In addition, it was observed that the brittleness levels of all three lithologic rock groups had become lower with increases in the confining pressure grade. These findings confirmed that brittleness is an intrinsic property of rock, and the differences in brittleness may not be great when the lithology is consistent and the compositions are similar. It was also proven that confining pressure levels inhibited the brittleness characteristics of the rock to a certain degree.

3.2.2 Verification and Analysis of the Brittleness of Granite Under Different Overburden Conditions

In the present study, triaxial compression tests were carried out on granite specimens with overburdens of 150 m, 300 m, 450 m, and 600 m, respectively. The stress–strain curves and the failure morphology of the rock samples are detailed in Fig. 6. As can be seen in the stress–strain curves of the uniaxial compression tests, the strength levels of the granite samples under different burial depths were all approximately 100 MPa, and had instantaneously dropped to approximately 0 MPa after the stress reached the peak. However, under the effects of confining pressure, it was observed that the granite exhibited both strength and peak strain increases, and also displayed a certain residual strength. Therefore, from the perspective of the failure morphology, it was found that the granite samples were mainly characterized by tensile failures under uniaxial compression, with generally three or more vertical splitting cracks formed. Furthermore, after the failures occurred, more debris was generated, indicating strong brittleness characteristics. The characteristic stress and strain values which were determined from the test curves are shown in Table 3. This study's comparison of the brittleness calculation results of the examined rock specimens is detailed in Fig. 7. The obtained triaxial test results demonstrated that the brittleness of granite at the same overburden decreased with increases in confining pressure. These findings had fully conformed with the above-mentioned analysis results of the stress–strain curves and failure morphology. In addition, it can be seen in the figure that under the same confining pressure, the overburden of the granite in 300 m, 450 m, and 600 m, respectively, displayed the phenomenon of gradually decreasing brittleness. However, the granite with a depth of 150 m had not satisfied the aforementioned rule. Therefore, it was considered that the influence effects of the overburden on rock brittleness should be further examined from the following three aspects: rock mineral composition; rock mass weathering degree; and differences in the internal structures of the rock.

It can generally be seen with the naked eye that the internal mineral particle sizes of granite tend to vary at different depths. Therefore, they can be effectively identified by polarizing microscopy, and their internal mineral compositions, microscopic particle structures, and particle sizes can be easily obtained. This study's test results and preliminary analyses are shown in Fig. 8 and Table 4. The results show that the granite was mainly composed of minerals such as quartz, feldspar, and mica. The quartz was a colorless and transparent crystal with no cleavage, and some of
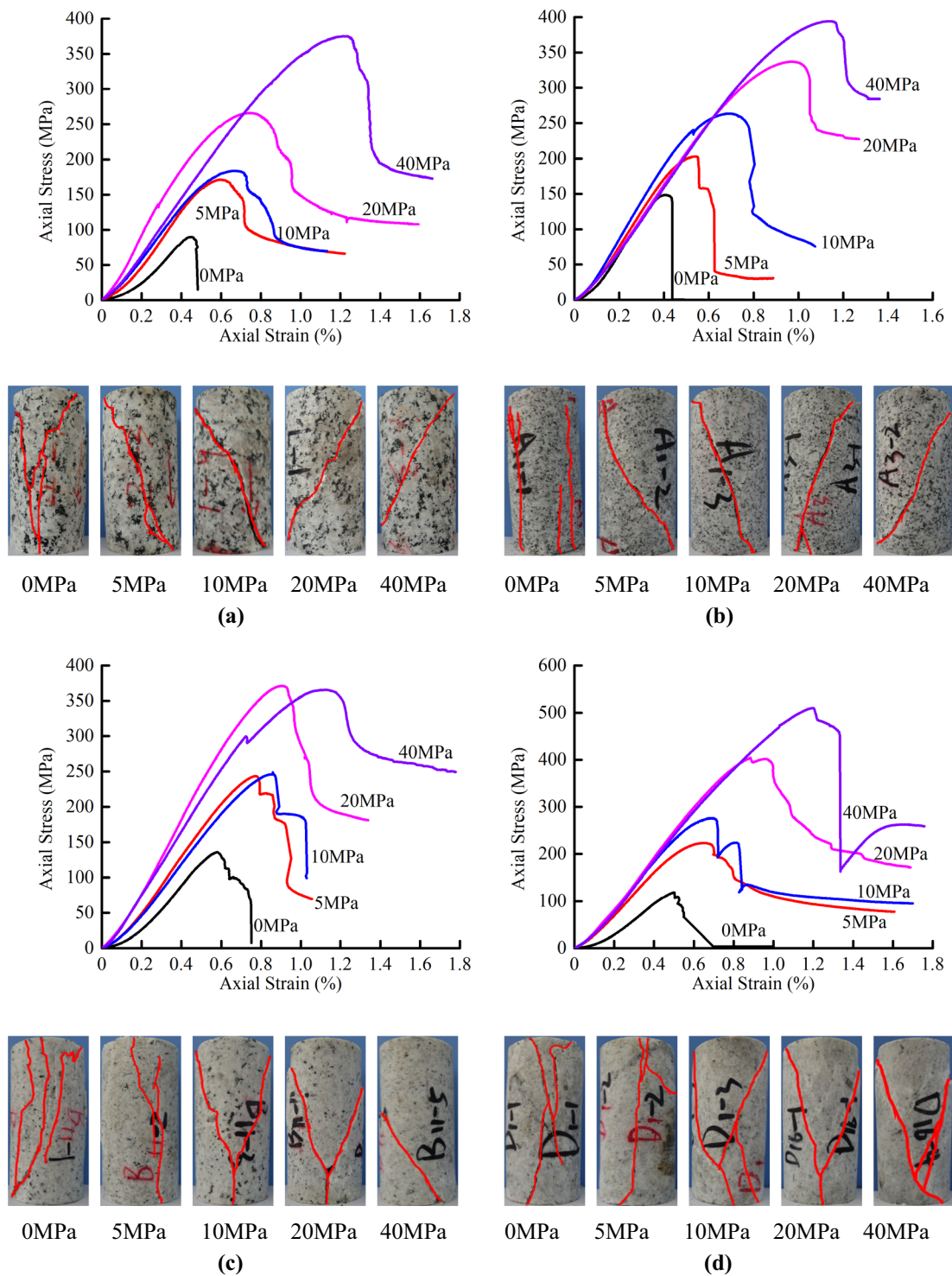
Fig. 6 Stress–strain curves and failure morphology of the granite triaxial compression tests under different overburden, in which **a–d** shows the test curves and failure morphology of the granite samples under the overburden of 150 m, 300 m, 450 m, and 600 m, respectively

it exhibited undulatory extinction. The feldspar had a lath-like shape, and the polysynthetic twin and carlsbad-al bite compound twin could be observed. The monomers of twins were relatively fine, and there were small mica inclusions,

with weak sericitization and carbonatization. The biotite bore obvious brown red-yellowish brown pleochroism, and a set of complete cleavage could be observed on the surface of biotite in granite thin section with buried depth of 150 m and

Table 3 Results of the triaxial compression tests of the rock samples under different overburden conditions

Overburden (m)	σ_3 (MPa)	σ_{ci} (MPa)	ε_{ci} (10^{-3})	σ_p (MPa)	ε_p (10^{-3})	σ_r (MPa)	ε_r (10^{-3})	BICSS
150	0	24.947	0.960	89.593	4.468	15.257	4.817	0.335
	5	41.816	0.805	171.315	4.817	94.223	7.747	0.205
	10	50.714	0.587	183.848	6.666	87.873	8.812	0.137
	20	61.702	0.597	266.182	7.432	118.969	12.160	0.113
	40	57.497	0.546	374.939	12.323	185.419	14.642	0.095
300	0	31.233	0.679	148.326	4.062	0.550	4.375	0.574
	5	45.880	0.556	202.678	5.359	40.568	6.463	0.427
	10	43.403	0.451	263.596	6.829	86.282	10.005	0.222
	20	41.656	0.470	336.983	9.681	262.579	10.518	0.169
	40	44.841	0.394	394.249	11.329	264.869	13.151	0.114
450	0	14.143	0.710	135.825	5.808	7.349	7.514	0.245
	5	38.095	0.658	243.539	7.711	69.503	10.553	0.172
	10	55.844	0.868	248.951	8.587	99.000	10.298	0.162
	20	70.345	0.537	370.998	9.042	181.346	13.385	0.124
	40	49.856	0.488	365.546	11.209	289.889	12.790	0.080
600	0	27.085	1.048	118.001	4.987	3.448	7.883	0.203
	5	35.790	0.417	223.231	6.464	113.083	9.744	0.154
	10	52.100	0.470	275.631	6.855	105.908	12.626	0.140
	20	82.663	0.429	403.382	8.831	175.899	16.090	0.105
	40	74.852	0.583	509.654	11.899	256.512	18.413	0.077

In the table, σ_3 denotes the confining pressure; σ_{ci}, σ_p, σ_r and ε_{ci}, ε_p, ε_r represent the crack initiation stress, peak compressive strength, residual compressive strength, and the strain value of the corresponding stress, respectively
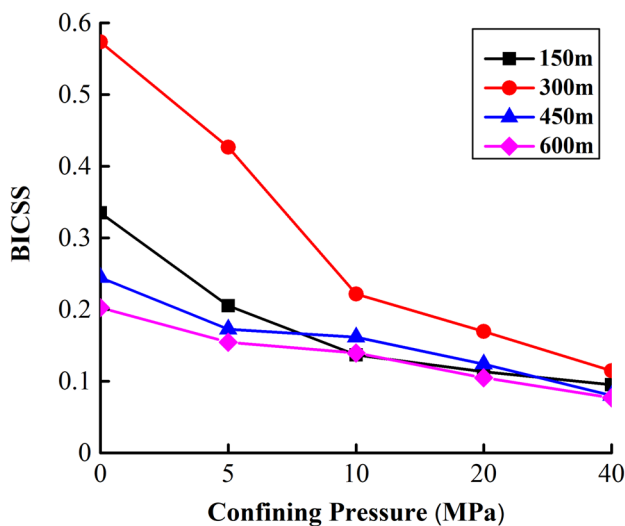

Fig. 7 Comparison of the brittleness indexes of different overburden granite specimens

the quartz particles displayed a multi-concentration inlaid distribution pattern. As seen from the surfaces of the specimens, the quartz particles were relatively complete, with only a few micro-cracks and particle sizes ranging between 0.20 and 4.20 mm. The quartz content was the second highest in the rock samples with burial depths of 600 m, and the particle sizes were the largest among the four burial depths, ranging from 0.40 to 5.20 mm. However, the majority of the particles had displayed suture-like mosaic distributions, and there were many cracks evident on the surfaces of the quartz. These findings indicated that, under the axial pressure, the actual stress at the crack tip of the quartz surface was far greater than the applied stress due to the stress concentration, which led to a great decrease in the strength of the specimen. The quartz content levels in the rock with an overburden of 300 m were found to be higher than that of the 450 m overburden, and the floating range of the quartz particle sizes in the rock with an overburden of 300 m was the smallest, ranging from 1.25 to 4.90 mm. Also, some cracks were observed on the quartz surfaces of both of the aforementioned rock, with geared mosaic distributions between the particles. However, there were no significant differences observed in the feldspar content levels structure between the above-mentioned granite specimens. Therefore, the influence effects on the rock brittleness were not significant.

300 m. Chloritization and carbonatization of biotite could be observed on the surface of biotite in granite thin section with buried depths of 300 m, 450 m, and 600 m, and the greater the burial depth was, the more obvious the alteration would be. As can be seen in the table, the quartz content of the granite with an overburden of 150 m was the highest, and
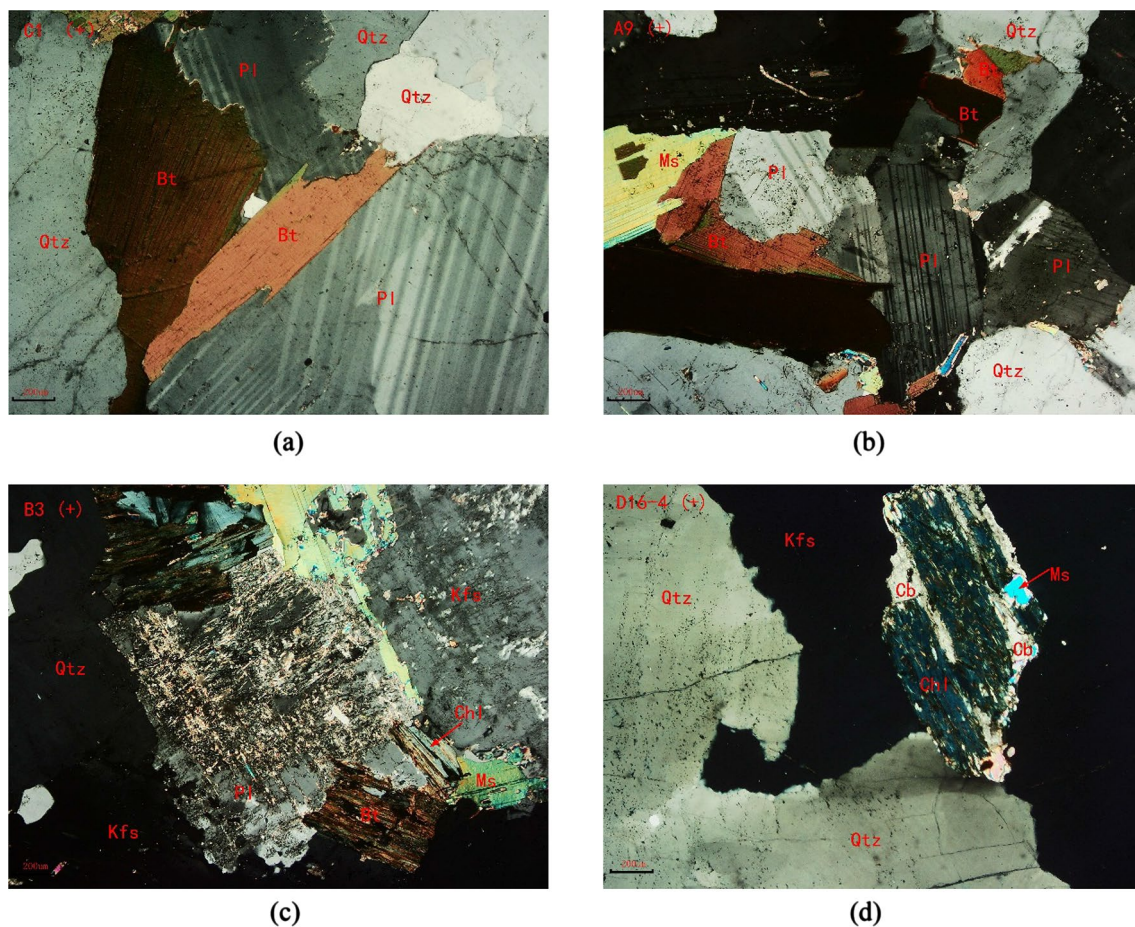
Fig. 8 Polarizing microscopic images of granite under different overburden, in which **a–d** show the polarizing microscope images of granite under the overburden of 150 m, 300 m, 450 m, and 600 m, respectively

Table 4 Description of the mineral characteristics of the granite under different overburden conditions

Overburden (m)	Mineral	Proportion (%)	Particle size (mm)	Morphology
150	Quartz	50	0.20–4.20	Anhedral crystal, granular
	Albite	45	0.80–4.40	hemimorphic crystal; lath-liked
	Biotite	3	0.45–2.40	schistose
	Magnetite	2		granular
300	Quartz	35–40	1.25–4.90	Anhedral crystal, granular
	Albite	50	0.65–3.25	hemimorphic crystal, lath-liked
	Biotite	15	0.20–1.25	schistose
450	Quartz	25	0.40–3.50	Anhedral crystal, granular
	Labradorite	40	0.90–5.60	subhedral-allotriomorphic crystals, lath-shaped, granular
	Albite	25	0.50–4.10	hemimorphic crystal, lath-liked
	Biotite	10	0.30–1.25	schistose
600	Quartz	40	0.40–5.20	Anhedral crystal, granular
	Labradorite	40–45	1.20–7.10	subhedral-allotriomorphic crystals, lath-shaped, granular
	Albite	5–10	0.20–1.25	Mainly to the subhedral-allotriomorphic crystals, lath-shaped, granular
	Biotite	8	0.15–2.20	schistose
	Dolomite	2	0.05–0.90	Irregular granular

It is likely that the presence of larger brittle grains in granite contributed to a more rapid cohesion loss rate (with straining) and slower frictional strengthening (Hajiabdolmajid and Kaiser 2003). In addition, the degree of internal occlusion between the quartz particles would also have a greater impact on the strength of the granite. It was found that under low confining pressure conditions, the brittleness of rock was mainly determined by the content levels of brittle minerals, particle sizes, and the degree of bonding between the particles. However, it was observed that, with increases in confining pressure, the influence effects of bonding between the particles rapidly decreased. Although it was found that the burial depths of 150 m and 300 m for the granite had resulted in only minor differences in the total content and the cementation structures of the quartz and feldspar, the particle sizes of the quartz particles in the rock with a burial depth of 300 m were larger and characterized with more concentrated size distributions. Therefore, under the condition of low confining pressure, it was concluded that the energy stored in the brittle minerals inside the rock was greater than that in the rock with a burial depth of 150 m, and the degree of brittle failure was also greater than that of the granite with an overburden of 150 m. Therefore, under the condition of low confining pressure (0.5 Mpa), the aforementioned special phenomenon in the evaluation results could be explained from the perspective of the influencing effects of the mineral particles in rock and the cementation structures between the particles.

Although the results of the polarizing microscopy showed that there were little differences in the content of the mineral components between the granite at different burial depths, it is noteworthy that the content of mica in granite with a 150 m burial depth was relatively low. This was due to the fact that mica is an unstable mineral and greatly affected by weathering. Therefore, this study preliminarily concluded that one of the special reasons may have been the weathering degrees of the rock specimens. The weathering degree of rock can be tested using wave velocity meters. In this study, six granite specimens were taken from each overburden level for the wave velocity testing processes. After eliminating the maximum and minimum values, the average wave velocity of the rock under different burial depths was obtained. It was observed that although the mineral compositions and content levels of the granite at the four burial depth levels were basically the same, their mechanical responses were quite different. Therefore, it was assumed that the homogeneity of the rock would eventually display the stiffness or strength characteristics of the rock. Therefore, the stiffness heterogeneity factor (SHF) proposed by Qiu et al. (2011) was adopted to quantify the homogeneity of the rock samples in this study. For example, when calculating the granite heterogeneity factors, the rock mineral stiffness parameters were adopted, and the stiffness parameters K_i of the various minerals were obtained according to the research results presented by Bass (1995). The calculation results of the heterogeneity factors and the rock wave velocity tests are shown in Table 5 and Fig. 9.

It can be seen from the table that in terms of the weathering degrees, the average wave velocities of granite with
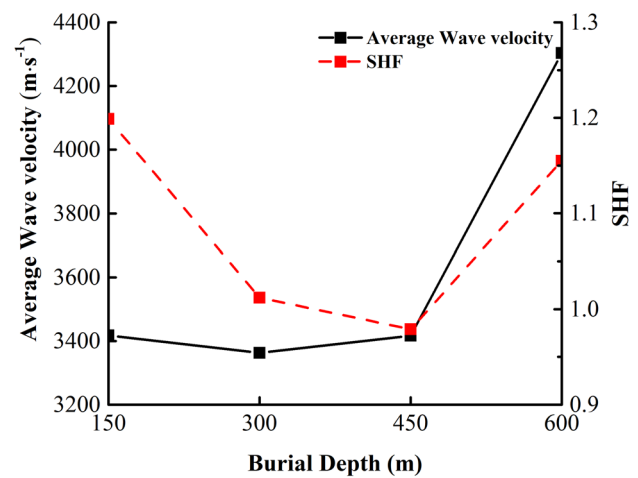

Fig. 9 Comparison of the SHF and wave velocities of granite under different overburden

Table 5 Stiffness homogeneity and wave velocity test results of the granite under different overburden conditions

Overburden (m)	150		300		450			600	
Wave velocity (m/s)	3070.62		3064.35		3393.67			4464.29	
	3880.98		3278.69		4032.26			4172.46	
	4261.36		3468.21		2881.84			4297.99	
	2457.00		3640.78		3359.46			4279.60	
Average value (m/s)	3417.49		3363.01		3416.81			4303.59	
SHF	1.199		1.012		0.979			1.155	
Mineral composition	Quartz	Albite		Labradorite	Dolomite	Muscovite			Magnetite
Mineral stiffness[a] (GPa)	37.8	56.9		74.5	94.9	58.2			161

In the table, [a]indicates the stiffness values of each mineral which were obtained in this study by referring to the reports presented by Bass (1995)

Table 8 Statistical characteristics of the stress and strain parameters of the granite

Rock type	Variables	Mean μ	Standard deviation σ	Distribution type
Granite	σ_{ci} (MPa)	45.456	7.02	Normal distribution
	ε_{ci} (10^{-3})	0.602	0.165	Normal distribution
	σ_p (MPa)	226.599	37.848	Normal distribution
	ε_p (10^{-3})	6.661	1.196	Normal distribution
	σ_r (MPa)	87.055	22.983	Normal distribution
	ε_r (10^{-3})	9.531	1.875	Normal distribution

burial depths of 150 m, 300 m, and 450 m were not large. Meanwhile, the wave velocity of the granite with an overburden of 600 m was found to be much larger. The sound waves propagated faster between the upper and lower surfaces of the granite at a depth of 600 m, which indicated that it had the lowest degree of weathering. In addition, from the perspective of rock homogeneity, the granites3 at the depths of 300 m and 450 m were the best in terms of homogeneity, while the granite at a depth of 150 m displayed the worst homogeneity characteristics. Therefore, in accordance with the comprehensive weathering degrees and homogeneity indexes of the examined rock, the granite at the 150 m depth not only had a higher degree weathering than that under the other burial depth grades, but also poor homogeneity.

Therefore, from the above-mentioned two aspects, it was concluded that the problems in the calculation results could be adequately explained.

4 Discussion

4.1 Analysis of the Indicator Universality

Through the analysis in the previous section, it is very reliable to use BICSS to evaluate the brittleness of rock in this project. However, the reliability of this index in the brittleness evaluation of rocks in different areas remains to be investigated. Therefore, this section will verify the universality of BICSS using the rock brittleness evaluation results of existing studies.

In this section, the authors have decided to use the test data of marble under different confining pressure levels and the test data of five different samples under the same test conditions described in Chen et al. (2019), to verify BICSS. The test data and brittleness index calculation results can be seen in Tables 6, 7, and Fig. 10.

As can be seen, the evaluation results of BICSS are completely consistent with the conclusions of this paper, whether studying the sensitivity of marble brittleness to confining pressure, or comparing the brittleness of different

Table 9 Parameter sensitivity analysis results

Variable	σ_{ci} (MPa)	ε_{ci} (10^{-3})	σ_p (MPa)	ε_p (10^{-3})	σ_r (MPa)	ε_r (10^{-3})
α	0.123	0.086	1.349	0.613	0.452	19.463

In the table, σ_{ci}, σ_p, σ_r and ε_{ci}, ε_p, ε_r represent the crack initiation stress, peak compressive strength, residual compressive strength, and the strain value of the corresponding stress, respectively
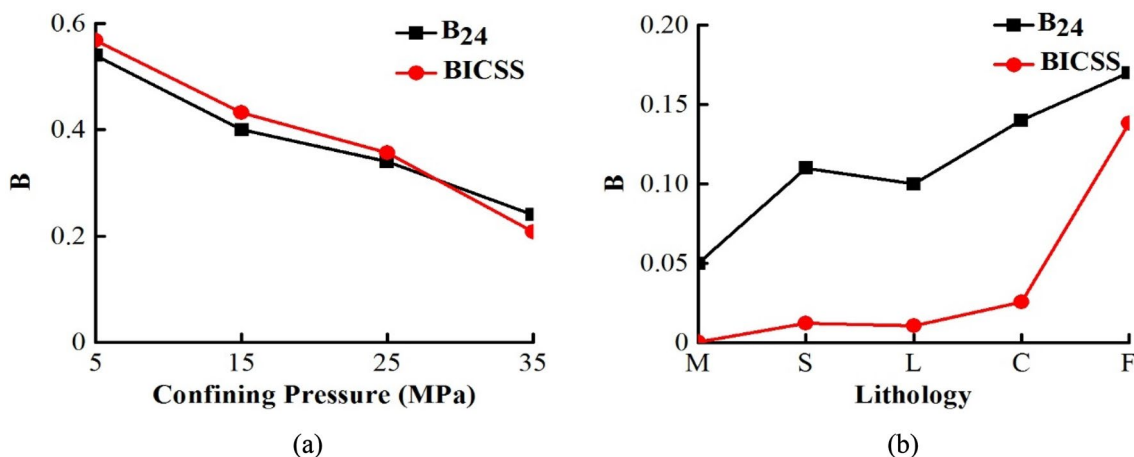

Fig. 10 Variation of the brittleness index: **a** the variation of brittleness index of marble under different confining pressure levels; **b** five different samples under the same confining pressure of 30 MPa

lithological rocks under the same test conditions. Therefore, the universality of BICSS was verified.

4.2 Parameter Sensitivity Analysis

Brittleness is a very important property of rock. It may be influenced by such internal factors as mineral compositions, particles sizes, structural characteristics, and cementing material. In addition, it may also be influenced by such external factors as weathering degrees, stress conditions, temperatures, and humidity. When comparisons were made of the brittleness characteristics of different lithologic rock, the brittleness was found to be mainly influenced by the intrinsic factors, such as mineral compositions, particle sizes, and structural characteristics of the rock. Meanwhile, the external factors, such as the temperature and humidity levels, were often observed to be equal under controlled laboratory testing conditions. In addition, when evaluating the brittleness of rock with the same lithology but different burial depths, it was found that the brittleness was mainly affected by the particle sizes, structural characteristics, and weathering degrees of the rock. The characteristic stress–strain values in the stress–strain curves obtained from uniaxial and triaxial laboratory testing processes were found to comprehensively reflect the influence effects of those factors on the rock brittleness. However, when the crack volume strain inflection point method proposed by Martin (1997) was used to determine the crack-initiation stress levels, due to the fact that the selections of the linear elasticity stage in the curves had varied from person to person, the solved crack-initiation stress and strain values were found to be different. Since the differences were expected to lead to differences in the rock brittleness results calculated by BICSS, a parameter sensitivity analysis of the BICSS was carried out to determine the potential influences of the aforementioned brittleness evaluation errors.

It has been found that under normal circumstances, to obtain accurate probability distribution models of the mechanical parameters rock masses, along with the statistical characteristic parameters, it is first necessary to obtain data samples of rock mass mechanical parameters through field or indoor testing processes. Then, for larger samples (sample sizes greater than 30), classical theoretical distribution methods are used to fit the probability distributions of the rock mechanic parameters, and $K - S$, Chi-square tests are utilized to test of goodness of fit. However, for limited small field samples, classical curve fitting methods, finite comparison methods, and Bayesian estimation methods can be used to infer the probability distributions of rock mass mechanical parameters (Li and Gong 2007). Then, the statistical characteristic parameters, such as the mean and standard deviations of the rock mass mechanical parameters, can be determined. In the present study, due to the lack of a large number of indoor data test samples under the same confining pressure, it was assumed that all the random variables obeyed the lognormal distribution. The data regarding the granite under the confining pressure levels of 5 MPa and 10 MPa were analyzed. The statistical characteristics of the characteristic stress–strain parameters are shown in Table 8.

There were three main steps in this study's parameter sensitivity analysis process:

1. A selection was made of the parameter values of the mean plus or minus twice the standard deviation in the vicinity of the mean value of each random variable. Then, six random variables for a total of 12 sets of parameters, plus a set of mean parameters, for a total of 13 sets of parameters, were identified;
2. Then, the 13 groups of parameters were taken into the BICSS to calculate the rock brittleness and extract the i-group random variables to obtain the parameter group calculation results BI_0, BI_1, and BI_2;
3. Finally, the parameter sensitivity index $\alpha = \left| (BI_1 - BI_2) \right| / BI_0$ was calculated.

It was found that the larger the parameter sensitivity index α was, the greater the influence effects of this parameter on the brittleness evaluation results would be. The calculation results of the sensitivity index are shown in Table 9. It can be seen in the table that the residual strain value had the greatest influence on the calculation results, which had conformed with the definition of brittleness as the magnitude of irrecoverable strain after material failure. However, the changes in the stress–strain values of the cracking actions

Table 6 Results of the triaxial compression tests of marbles (Chen et al. 2019)

Confining pressure (MPa)	σ_{ci} (MPa)	ε_{ci} (10^{-3})	σ_p (MPa)	ε_p (10^{-3})	σ_r (MPa)	ε_r (10^{-3})	B_{24}	BICSS
5	87.93	1.69	192.08	3.73	71.96	5.98	0.54	0.5674
15	89.35	1.59	258.75	4.87	123.94	7.43	0.4	0.4320
25	116.04	1.97	297.07	5.61	162.81	8.17	0.34	0.3571
35	126.05	1.94	332.89	6.39	190.99	10.72	0.24	0.2074

In the table, σ_{ci}, σ_p, σ_r and ε_{ci}, ε_p, ε_r represent the crack initiation stress, peak compressive strength, residual compressive strength, and the strain value of the corresponding stress, respectively

Table 7 Results of the triaxial compression tests of different rock samples (Chen et al. 2019)

Lithology	σ_{ci} (MPa)	ε_{ci} (10^{-3})	σ_p (MPa)	ε_p (10^{-3})	σ_r (MPa)	ε_r (10^{-3})	B_{24}	BICSS
Marble	75.92	1.52	134.52	11.24	126.54	24.34	0.05	0.0003
Sandstone	106.05	3.60	245.68	11.38	144.48	21.57	0.11	0.0122
Limestone	248.16	9.67	286.09	12.77	198.06	18.39	0.10	0.0106
Coarse-grained granite	120.90	3.79	291.09	11.23	133.42	20.60	0.14	0.0257
Fine-grained granite	145.19	1.93	476.75	8.80	9.72	22.21	0.17	0.1380

In the table, σ_{ci}, σ_p, σ_r and ε_{ci}, ε_p, ε_r represent the crack initiation stress, peak compressive strength, residual compressive strength, and the strain value of the corresponding stress, respectively

were observed to be less affected by the entire brittleness calculation results. Therefore, it was concluded in this study that the small differences in the crack initial stress and strain values caused by human error factors would not have major influences on the entire calculation results.

5 Conclusions

Accurate evaluations of rock brittleness are very important for the safety and stability of underground engineering processes. This study examined and analyzed the existing brittleness indexes, and then theoretically proposed a brittleness evaluation method (BICSS) based on the complete stress–strain curves of rock. Conventional triaxial tests were completed on metamorphic sandstone, granite, and gneiss specimens. In addition, wave speed tests were performed on the granite, and polarizing microscopy and other testing methods were adopted, to verify the reliability of the proposed index. Subsequently, the internal and external influencing factors of rock brittleness were further revealed. The adaptability of BICSS to rock brittleness evaluation in different areas was discussed, and the influence of each parameter change on the final evaluation result was analyzed. The main conclusions reached in this study were as follows:

1. Combining the definition of brittleness and the failure mechanism of rock materials, it is proposed that the study of the whole process from the initiation of cracks to the complete loss of bearing capacity is helpful to better describing the brittleness of rock. Therefore, this paper establishes a new rock brittleness evaluation method BICSS. The method was based on the complete stress–strain curves of rock, considering not only the stress rise rates from the crack-initiation stage to the peak failure, but also the stress drop rates from the peak failures to the residual points. Finally, the strain values at the peak points were taken into account as controlling factors. The feasibility of the index is proven by theoretical analysis.

2. Conventional triaxial tests were performed on metamorphic sandstone, granite, and gneiss in a group of deep-buried long-line tunnels. Through the analysis of test curves and rock failure morphology, the brittle relationship of the three rocks was determined to be as follows: metastone > granite > gneiss. Under the condition of the same lithology yet different confining pressure levels, three kinds of specimens all show obvious confining pressure effect; in other words, the brittleness of specimens is inversely proportional to the confining pressure applied. The typical brittleness indexes and BICSS are used to evaluate and compare the brittleness of rocks. The results show that, under uniaxial conditions, all brittleness indexes can basically distinguish the brittleness of different lithological rocks. Under the condition of triaxial compression, the evaluation results of typical brittleness indexes have either greater or lesser deviation from the analysis results in this paper, whereas BICSS can match the analysis results more closely.

3. Following the confirmation of the applicability and reliability of the BICSS, the brittleness levels of granite specimens under different overburdens were evaluated. The evaluation results show that the brittleness of granite under the same overburden decreases with the increase of confining pressure. However, for the brittleness comparison of specimens with different overburden under the same test conditions, it was found that the brittleness of granite with a depth of 150 m under the confining pressure values of 10 MPa and 20 MPa was unique. In view of this phenomenon, the polarizing microscope identification tests and acoustic wave tests, and mineral homogeneity calculations were completed for rock specimens under different burial depths. The reason for the aforementioned phenomenon was reasonably explained from the perspectives of rock mineral composition, size distribution of mineral particles, degree of internal occlusion between particles, rock stiffness heterogeneity, and degree of weathering.

4. Observing the test data in the article of brittleness index B_{24}, i.e., the test data of marble under different confining pressures and those of five different samples under the same test conditions to verify the universality of BICSS, it is seen that the evaluation results of BICSS are consistent with the conclusions in the author's article, which

proves that BICSS can be applied to evaluate the brittleness of rock under different engineering background conditions.

5. This research study performed a parameter sensitivity analysis of the proposed BICSS. The results showed that BICSS was the most sensitive to the residual strain values of which the parameter sensitivity index is $\alpha=19.463$, followed by the peak stress and strain values. Meanwhile, the effects of the crack-initiation stress and strain values were not significant, wherein the parameter sensitivity indexes were $\alpha=0.123$ and $\alpha=0.086$, respectively, thereby negating the influence effects of the observed small differences in the crack-initiation stress and strain values in the overall calculation results caused by human error factors.

References

Altindag R (2002) The evaluation of rock brittleness concept on rotary-blast hold drills. J South Afr Inst Min Metall 102:61–66

Altindag R (2008) Relationships between brittleness and specific energy in excavation mechanics. In: Proceedings of 9th regional rock mechanics symposium. Izmir, Turkey, pp 437–451

Bass JD (1995) Elasticity of minerals, glasses, and melts. Miner Phys Crystallogr A Handb Phys Constants 2:45–63

Bishop AW (1967) rogressive failure with special reference to the mechanism causing it. In: Proceedings of the Geotechnical Conference, Oslo, Norway, pp 142–150, 523–527

Buller D, Hughes S, Market J, Petre E (2010) Petrophysical evaluation for enhancing hydraulic stimulation in horizontal shale gas-wells. In: SPE annual technical conference and exhibition held in Florence, Italy, SPE 132990

Chen GQ, Zhao C, Wei T et al (2018) Evaluation method of rock brittleness characteristics based on total stress-strain curve and initiation stress. Chin J Rock Mech Eng 37(1):51–59

Chen GQ, Jiang W, Sun X et al (2019) Quantitative evaluation of rock brittleness based on crack-initiation stress and complete stress–strain curves. Bull Eng Geol Env 2019:9

Coates DF, Parsons RC (1966) Experimental criteria for classification of rock substances. Int J Rock Mech Min Sci Geomech Abstr 3:181–189

Fairhurst CE, Hudson JA (1999) Draft ISRM suggested method for the complete stress-strain curve for intact rock in uniaxial compression. Int J Rock Mech Min Sci Geomech Abstr 36(3):281–289

Gautam PK, Verma AK, Jha MK et al (2016) Study of strain rate and thermal damage of dholpur sandstone at elevated temperature. Rock Mech Rock Eng 49:3805–3815

Gautam PK, Verma AK, Jha MK et al (2018) Effect of high temperature on physical and mechanical properties of jalore granite. J Appl Geophys 159:460–474

Gautam PK, Jha MK, Verma AK, Singh TN (2019) Experimental study of thermal damage under compression and tension of makrana marble. J Therm Anal Calorimetry 2019:3

George EA (1995) Brittle failure of rock material—test results and constitutive models. In: A. A. Balkema, Rotterdam, pp 123–128

Hajiabdolmajid V, Kaiser PK (2003) Brittleness of rock and stability assessment in hard rock tunneling. Int J Tunn Undergr Space Technol 18(1):35–48

Hetenyi M (1950) Handbook of experimental stress analysis. Wiley, New York

Howell JV (1960) Glossary of geology and related sciences. American Geological Institute, Washington, DC

Hucka V, Das B (1974) Brittleness determination of rocks by different methods. Int J Rock Mech Min Sci Geomech Abstr 11(10):389–392

ISRM (1983) Suggested methods for determining the strength of rock materials in triaxial compression: revised version. Int J Rock Mech Min Sci Geomech Abstr 20(6):285–290

Jarvie DM, Hill RJ, Ruble TE, Pollastro RM (2007) Unconventional shale-gas systems: the Mississippian Barnett Shale of northcentral Texas as one model for thermogenic shale-gas assessment. AAPG Bull 9(4):475–499

Komurlu E (2018) Loading rate conditions and specimen size effect on strength and deformability of rock materials under uniaxial compression. Int J Geo-Eng 9:1

Li XB, Gong FQ (2007) A research review of the method to deduce the probability distribution of geotechnical mechanics parameters. J Changsha Univ Sci Technol Natural Sci 4(1):1–8

Li QH, Chen M, Jin Y (2012) Rock mechanical properties and brittleness evaluation of shale gas reservoir. Chin J Pet Drill Tech 40(4):17–22

Martin CD (1997) The effect of cohesion loss and stress path on brittle rock strength. Can Geotech J 34(5):698–725

Meng F, Zhou H, Zhang C, Xu R, Lu J (2015) Evaluation methodology of brittleness of rock based on post-peak stress–strain curves. Rock Mech Rock Eng 48(5):1787–1805

Meng Q, Zhang M, Han L, Pu H, Li H (2016) Effects of size and strain rate on the mechanical behaviors of rock specimens under uniaxial compression. Arab J Geosci 9(8):527

Morley A (1944) Strength of Materials: with 260 diagrams and numerous examples. Longmans, Green and Company, New York

Obert L, Duvall W (1967) Rock mechanics and the design of structures in rock. Wiley, New York

Qiu SL, Feng XT, Zhang CQ et al (2011) Establishment and verification of rock burst liability index RVI of deep buried hard rock tunnel. Chin J Rock Mech Eng 30(6):1

Ramsey J (1968) Folding and fracturing of rock. McGraw-Hill, New York

Rickman R, Mullen M J, Petre J E, et al (2008c) A practical use of shale petrophysics for stimulation design optimization. In: All shale plays are not clones of the Barnett Shale; proceedings of the SPE 115258; Proc Ann Tech Conf, Denver, Co,USA, pp, F, Society of Petroleum Engineers

Tarasov BG, Potvin Y (2012) Absolute, relative and intrinsic rock brittleness at compression. Min Technol 121:4

Tarasov B, Potvin Y (2013) Universal criteria for rock brittleness estimation under triaxial compression. Int J Rock Mech Min Sci 2013:59

Wang FP, Gale JF (2009) Screening criteria for shale-gas systems. Gulf Coast Assoc Geol Trans 59:779–793

Wang Y, Li X, Wu YF et al (2014) Research on relationship between crack-initiation stress level and brittleness indices for brittle rocks. Chin J Rock Mech Eng 33(2):264–275

Xia YJ, Li LC, Tang CA et al (2017) A new method to evaluate rock mass brittleness based on stress–strain curves of class I. Rock Mech Rock Eng 50:1123–1139

Yagiz S (2009) Assessment of brittleness using rock strength and density with punch penetration test. Tunn Undergr Space Technol 24(1):66–74

Yang SQ, Su CD, Xu WY (2005) Experimental and theoretical study of size effect of rock material. Chin J Rock Mech Eng 22(112):118

Zhang HJ, Li CC (2019) Effects of confining stress on the post-peak behaviour and fracture angle of fauske marble and iddefjord granite. Rock Mech Rock Eng 52(5):1377–1385